# Combretastatin A4 Phosphate Has Tumor Antivascular Activity in Rat and Man as Demonstrated by Dynamic Magnetic Resonance Imaging

By Susan M. Galbraith, Ross J. Maxwell, Martin A. Lodge, Gillian M. Tozer, John Wilson, N. Jane Taylor, J. James Stirling, Luiza Sena, Anwar R. Padhani, and Gordon J.S. Rustin

***Purpose:*** **Combretastatin A4 phosphate (CA4P) is a novel vascular targeting agent. Dynamic contrast enhanced magnetic resonance imaging (DCE-MRI) studies were performed to examine changes in parameters related to blood flow and vascular permeability in tumor and normal tissue after CA4P treatment.**

***Materials and Methods:*** **Changes in kinetic DCE-MRI parameters (transfer constant [$K^{trans}$] and area under contrast medium-time curve [AUC]) over 24 hours after treatment with CA4P were measured in 18 patients in a phase I trial and compared with those obtained in the rat P22 carcinosarcoma model, using the same imaging technique. Rats were treated with 30 mg/kg of CA4P; patients received escalating doses from 5 to 114 mg/m$^2$.**

***Results:*** **A similar pattern and time course of change in tumor and normal tissue parameters was seen in rats and humans. Rat tumor $K^{trans}$ was reduced by 64% 6 hours after treatment with CA4P (30 mg/kg). No significant reductions in kidney or muscle parameters were seen. Significant reductions were seen in tumor $K^{trans}$ in six of 16 patients treated at ≥ 52 mg/m$^2$, with a significant group mean reduction of 37% and 29% at 4 and 24 hours, respectively, after treatment. The mean reduction in tumor initial area under the gadolinium–diethylenetriamine pentaacetic acid concentration-time curve (AUC) was 33% and 18%, respectively, at these times. No reduction was seen in muscle $K^{trans}$ or in kidney AUC in group analysis of the clinical data.**

***Conclusion:*** **CA4P acutely reduces $K^{trans}$ in human as well as rat tumors at well-tolerated doses, with no significant changes in kidney or muscle, providing proof of principle that this drug has tumor antivascular activity in rats and humans.**

***J Clin Oncol 21:2831-2842.*** 

THE COMBRETASTATINS are a group of compounds isolated from the South African tree, *Combretum caffrum*.[1] They have a similar structure to that of colchicine, and bind to the colchicine-binding site on tubulin,[2] causing depolymerization of microtubules. Combretastatin A4 (CA4) is one of the most potent of these compounds,[3] and its disodium phosphate is a more water-soluble prodrug,[4] which is rapidly converted by nonspecific endogenous phosphatases into combretastatin A4 phosphate (CA4P). Its selective tumor vascular targeting action has been demonstrated in vivo and in an ex vivo isolated tumor perfusion system.[5,6] In P22 carcinosarcomas in rats, a 100-fold decrease in tumor blood flow was seen at 6 hours after a high dose of CA4P (100 mg/kg), with a much smaller reduction in blood flow to spleen, skin, skeletal muscle, and brain. No significant reduction was observed in heart, kidney, and small intestine.[6] Similar effects were found in the rat soon after administration of lower CA4P doses (10 and 30 mg/kg), but recovery of tumor blood flow occurred after 24 hours.[7]

The Cancer Research United Kingdom phase I trial of CA4P commenced in November 1998.[8] An integral part of this trial was an assessment of tumor microcirculation and blood flow using dynamic contrast medium enhanced magnetic resonance imaging (DCE-MRI) studies at Mount Vernon Hospital (Middlesex, United Kingdom) and positron emission tomography (PET) imaging with oxygen-15 ($^{15}O$)–labeled water at the Hammersmith Hospital (London, United Kingdom).[9] DCE-MRI is a noninvasive technique during which the tissue concentration of the paramagnetic contrast agent, gadolinium–diethylenetriamine pentaacetic acid (Gd-DTPA), is measured over several minutes from a series of T1-weighted images.[10] The change in Gd-DTPA concentration with time can be analyzed using pharmacokinetic models.[11] Gd-DTPA is neither freely diffusible nor a pure blood pool agent, and therefore the rate constant for the transfer of Gd-DTPA from the plasma into the extracellular space (transfer constant [$K^{trans}$]) will be affected by permeability changes as well as blood flow changes, although in highly permeable vessels such as those in tumors it approximates to the plasma flow per unit volume of tissue.[11] DCE-MRI techniques are able to characterize the microvascular response of tumors to a variety of physical and pharmaceutical treatments including chemotherapy, radiotherapy, and embolization.[12-16] We previously compared the DCE-MRI technique with tumor blood flow rate measurements using the uptake of radiolabeled iodoantipyrine (IAP) in the rat P22 carcinosarcoma model.[17] The time-course of changes in $K^{trans}$ and area under the Gd-DTPA

*From the Gray Cancer Institute, Paul Strickland Scanner Centre, Department of Medical Oncology, Mount Vernon Hospital, Northwood, Middlesex; and Cancer Research United Kingdom, Cambridge Terrace, London, United Kingdom.*

*Submitted May 29, 2002; accepted May 20, 2003.*

*Supported by grants from the Community Fund and Cancer Research United Kingdom. CA4P was supplied by OXiGENE, Inc, Watertown, MA.*

*Address reprint requests to Gordon J.S. Rustin, MD, Department of Medical Oncology, Mount Vernon Hospital, Northwood, Middlesex HA6 2RN, United Kingdom; email: rustin@mtvern.co.uk.*



*0732-183X/03/2115-2831/$20.00*


DOI: 10.1200/JCO.2003.05.187

concentration-time curve (AUC) as measured by DCE-MRI, and tumor blood flow rate as measured by IAP uptake after treatment with CA4P were similar, although the changes in $K^{trans}$ and AUC were smaller than those in blood flow rate. Thus, the use of DCE-MRI as a marker of change in tumor blood flow after CA4P leads to a relative underestimate of the size of the effect on blood flow rate, probably because of the contribution of changes in permeability to the values of $K^{trans}$ and AUC.

In this study, we measured the serial changes in DCE-MRI parameters in tumor, kidney, and muscle of cancer patients in the setting of a phase I clinical trial of CA4P. For comparison, we have carried out a similar study in rats that bear the P22 carcinosarcoma. In contrast to our previous rat study,[17] the magnetic resonance protocol used here was designed specifically to match closely that used in the clinical study. In particular, repeat examinations of individual animals were carried out and normal tissues, as well as tumors, were imaged. The purpose of the study was two-fold. First, we aimed to determine whether CA4P produces a measurable change in DCE-MRI parameters in human tumors and normal tissues, and examined the time-course of any changes. Second, because in vivo testing is a necessary and important step in preclinical development of vascular-targeted drugs, we aimed to evaluate the usefulness of the rat P22 carcinosarcoma in this regard.

## MATERIALS AND METHODS

### *Animal Studies*

*Tumor model.* Male rats bearing subcutaneously implanted P22 carcinosarcomas[18] on the flank were studied when the tumor diameter was approximately 16 mm. Animals were treated with CA4P in saline (30 mg/kg; OXiGENE, Inc, Watertown, MA) by intraperitoneal injection at approximately 3 mL/kg. Control rats received saline alone. MRI examination was carried out at 1, 6, and 24 hours after CA4P treatment, with serial measurements on individual animals. At least five rats were examined for each combination of treatment group and time point. Rats were anesthetized for tail vessel cannulation and MRI procedures using intraperitoneal injection of fentanyl citrate (0.32 mg/kg), fluanisone (10 mg/kg; both from Hypnorm, Janssen Animal Health, High Wycombe, United Kingdom), and midazolam (5 mg/kg; Hypnovel, Roche, Welwyn Garden City, United Kingdom). Additional anesthesia was used as required. Rat body temperature was maintained in the MRI apparatus using a recirculating warm water system.

*MRI.* Animals were examined in a 4.7-T, 30-cm-diameter, horizontal-bore magnet of an Inova MR spectroscopy imaging system (Varian, Palo Alto, CA). Rats were placed inside a 6.0-cm-diameter quadrature birdcage coil that was used as both transmitter and receiver. Animals were examined at either 30 minutes before injection of CA4P or saline and 24 hours after treatment, or at 30 minutes before and 1 and 6 hours after treatment.

Precontrast $T_1$ values were determined using an inversion recovery sequence. The sequence consisted of a 180° sync pulse followed by a variable interval, time of inversion period (150, 450, 1,000, or 2,500 ms), and then a spin echo period (time of echo period [TE], 10 ms) with 1-ms gaussian pulses. Other parameters included repetition time (TR), 2550 ms; slice thickness, 2 mm; field of view, 60 × 65 mm; and matrix size, 256 × 64 pixels. A set of four inversion recovery images was obtained for each tumor just before each injection of Gd-DTPA.

A set of 60 DCE gradient echo images were obtained with time resolution of 6.0 seconds per image. Five images were obtained before and the remainder after administration of contrast agent. The contrast agent, Gd-DTPA (Magnevist, Schering Health Care Ltd, Burgess Hill, United Kingdom), was administered at a dose of 0.1 mmol/kg in a volume of 1.0 mL/kg over 5 seconds via an infusion pump connected to a cannulated tail vein. MRI parameters used were TR, 60 ms; TE, 2.2 ms; flip angle 70°; slice thickness, 2 mm for three slices; field of view, 60 × 65 mm; and matrix size, 256 × 100 pixels (giving 0.24 × 0.65 mm in-plane resolution).

*Data analysis.* Animal MRI data were analyzed using a similar approach to that previously described for tumors in rats.[17,19] The analysis was made up of the following stages. (1) Tumor, muscle, and kidney regions of interest (ROIs) were outlined. (2) Segmentation of each ROI into up to eight subregions was performed on the basis of the signal intensity time course in individual pixels using an unsupervised neural network approach.[17,19] The subregions consist of clusters of pixels that have similar patterns of contrast agent kinetics. (3) $T_1$ values immediately before each injection of contrast agent were calculated for each tissue. (4) Gd-DTPA concentrations were estimated for each pixel on the basis of these $T_1$ values and the signal intensity values obtained during the dynamic MRI sequence. (5) The AUC for Gd-DTPA concentration-time for 0 to 90 seconds was calculated for individual pixels. Differential effects on tumor AUC were evaluated by calculating mean values for pixels in the periphery (< 2.0 mm from the edge) and from the center (> 5.0 mm from the edge). (6) The time course values of Gd-DTPA, $C_t(t)$, were fit to a model function that assumed a fixed arterial input function (AIF), $C_a(t)$,[20] for each cluster and for the entire ROI.

$$C_r(t) = K^{trans} \cdot C_a(t) \otimes \exp(-k_{ep} \cdot t) \quad (1)$$

where $K^{trans}$ is the transfer constant from the plasma to the extravascular extracellular space (EES), $\otimes$ is convolution, and $k_{ep}$ is the rate constant from the EES into plasma. (7) The leakage space, $v_e$, or volume of EES per unit volume of tissue was calculated from

$$v_e = K^{trans}/k_{ep} \quad (2)$$

Mathematical modeling of the kidney data to equation 1 gave poor fits because this model does not account for a vascular compartment. The parameter AUC was therefore used for these ROIs, and model parameters are not presented. Mean changes in parameters after treatment were compared with baseline using Student's paired *t* test.

### *Clinical Studies*

The local ethics committee approved the trial protocol, and all patients participating in this study gave written informed consent. CA4P was made up to 100 mL in normal saline, and delivered intravenously over 10 minutes via an infusion pump once a week for three doses, followed by a 1-week interval (three doses in 4 weeks comprised one cycle). A minimum of three patients was treated at each dose level. Initially, intrapatient dose escalation was allowed with dose doubling until at least grade 2 toxicity was seen. Subsequent dose escalations were 1.3-fold. At least one patient at each dose level was required to undergo DCE-MRI examination. Patients for DCE-MRI examination were selected on the basis of assessable disease at sites of little physiologic motion. DCE-MRI examinations were performed before treatment and at 24 hours after the first treatment at each dose level for the initial intrapatient escalation phase and 13 days after the third dose. The protocol was modified once intrapatient dose escalation was completed. Animal DCE-MRI data prompted an earlier MRI examination at 4 to 6 hours after the first dose of each cycle of three doses. An extra pretreatment MRI examination was added to determine the reproducibility of the technique. Blood pressure and heart rate were monitored every 30 minutes for the first 4 hours after each dose of CA4P.

*MRI.* The MRI methods have been reported previously and are summarized below.[21] The MRI studies were performed on a 1.5 T System, Magnetom Symphony (Siemens Medical Systems, Erlangen, Germany) using a body coil. At each scanning session, diagnostic images required for disease assessment were first obtained. A marker lesion (> 2 cm in size) was chosen for the DCE-MRI. An experienced radiographer repositioned the patient on serial visits, using internal bony landmarks such as disk spaces to minimize positioning errors. Between three and five slices were chosen up to 8 cm apart (with one slice through the center of the marker lesion), and the other slices were positioned to enable evaluation of kidney and skeletal

muscle, where possible. When tumors grew during the period of the examination, the same slice location was chosen and a note of a change in tumor size and configuration was made.

Proton density-weighted spoiled-gradient echo fast low angle shot (FLASH) images (TR, 350 ms; TE, 9.8 ms; flip angle, 20°; slice thickness, 10 mm; field of view 350 mm × 350 mm; and matrix size, 192 × 256 pixels) were then acquired at the same slice positions to enable the calculation of tissue Gd-DTPA concentration.[22] A dynamic series of 30 T1-weighted FLASH images was acquired for the same slice positions, with three images before a manual bolus intravenous injection of 0.1 mmol/kg Gd-DTPA, given over 10 to 12 seconds using a standardized injection protocol. Images were acquired consecutively with no time gaps. Each set of images took 11.9 seconds to acquire, and the whole sequence took 6 minutes. The imaging parameters for the T1-weighted FLASH sequence were TR, 80 ms; TE, 9 to 10 ms; flip angle, 70°; slice thickness, 10 mm; field of view 350 mm × 350 mm; and matrix size, 192 × 256 pixels. System gain and scaling factors were maintained between acquisition of the proton density and T1-weighted dynamic series of images.

Images were transferred to a Sun workstation (Sparc 10, Sun Microsystems, Mountain View, CA) and analyzed using Analyze software (Mayo Foundation, Rochester, MN). Information from anatomic T1- or T2-weighted images and postcontrast T1 images was used to draw ROIs carefully around the tumor edges, including the whole tumor where possible, but excluding pulsatility artifacts from blood vessels and susceptibility artifacts from adjacent bowel or bone. ROIs were also drawn for areas of skeletal muscle (usually paraspinal muscle) and around the renal cortex. Identical ROIs were used for each pretreatment examination and for posttreatment examinations at 4 and 24 hours after the first dose of CA4P. For patients in whom the tumor had changed in size on later examinations, a new ROI was drawn to encompass the entire tumor. Sizes of ROIs in normal tissues were unchanged. Errors relating to ROI placement were minimized by evaluating anatomic images by consensus review, by performing pre- and posttreatment kinetic analysis at the same sitting (thus reducing intraobserver variability), and by recording the exact sites of the ROIs.

Quantitative analysis required conversion of the MRI signal intensities to Gd-DTPA concentrations.[22] First, the longitudinal relaxation rate (T1) of the water protons at each time point in the dynamic T1-weighted sequence was obtained from the ratio of each T1-weighted image to the baseline proton density-weighted image in conjunction with data from a calibration experiment that involved phantoms with known T1 relaxation time values.[22] Initial measurements of T1 values of tissues in vivo using this protocol are consistent with T1 values at 1.5 T in the literature.[23] Gd-DTPA concentration, $C_t(t)$, was then inferred from the tissue T1 using the following equation:

$$C_t(t) = [1/\mathrm{T1}(t) - 1/\mathrm{T1}_0/\mathrm{r1} \quad (3)$$

where $T1_0$ is the tissue T1 without contrast and r1 is the longitudinal relaxivity of protons in vivo as a result of Gd-DTPA (taken to be 4.5 L/s/mmol at 1.5 T).[24] Quantitative modeling parameters including transfer constant ($K^{trans}$), rate constant ($k_{ep}$), and leakage space ($v_e$) were calculated by fitting a multicompartment model to the tissue contrast agent concentration-time curve[11,25] for each pixel in the ROI, and the results were presented as parametric pixel images. This model uses the same equation 1 as that used in the rat studies. An assumed AIF was used for the modeling procedure,[26] as described previously.[21] Nonenhancing pixels were defined as those in which there was no discernible Gd-DTPA measured above the baseline noise level, and includes pixels with $K^{trans}$ values lower than 0.001 mL/mL/min. These were assumed to represent nonviable (necrotic or fibrotic) areas. The percentage of nonenhancing pixels in each ROI was recorded.

In tissues with a large vascular volume fraction, such as kidney, the assumptions of our model that the contribution of intravascular Gd-DTPA to signal intensity is insignificant is not appropriate. Furthermore, there is active excretion of contrast medium. Therefore, for kidney, the AUC for Gd-DTPA concentration-time over the first 90 seconds was used.[25] The physiologic meaning of this parameter is less clear than that of $K^{trans}$, although the time course and extent of change in AUC were similar to those of $K^{trans}$ in our previous study,[17] and a good correspondence between $K^{trans}$ and AUC when mathematical simulations were used over a variety of AIFs has been reported elsewhere.[25] Tumor AUC values (using the same ROI as for $K^{trans}$ calculations) were also obtained for the purposes of comparison with kidney AUC results.

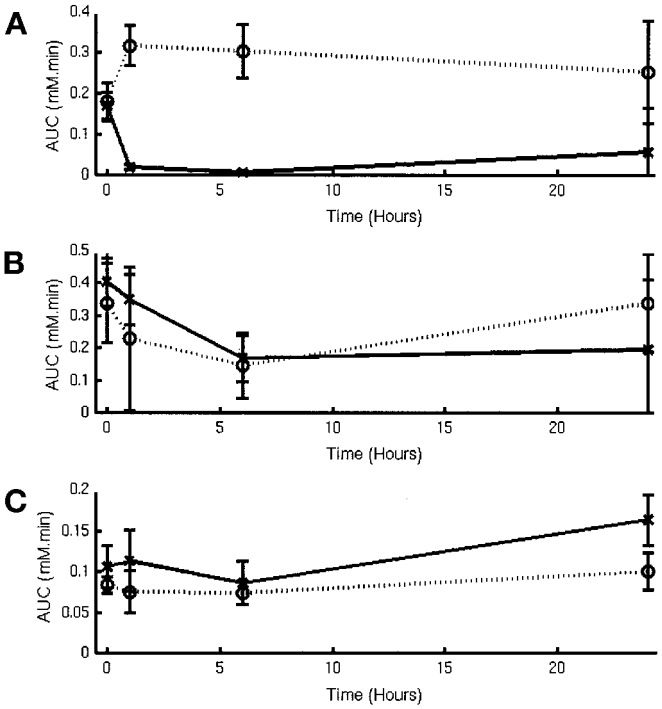


**Fig 1. Serial $K^{trans}$ parametric maps overlain on transverse T1-weighted images for patient 6, a 58-year-old female with metastatic leiomyosarcoma involving para-aortic lymph nodes, treated at 88 mg/m². The scale on the left of each image gives the values of $K^{trans}$ in mL/mL/min, which correspond to the colors displayed in each pixel. (Bottom) Corresponding T2-weighted anatomic image. Mean tumor $K^{trans}$ at baseline was 0.101 mL/mL/min and changed by −66%, −34%, −28%, and −72% at 4 hours after first dose, 24 hours after first dose, 13 days after third dose, and 13 days after sixth dose, respectively. Nonenhancing pixels formed 27% of tumor region of interest at baseline, and 88%, 27%, 14%, and 63% at the subsequent time points, respectively.**

Although the tumor tissue response was frequently heterogeneous, a single global value for the entire region was obtained by taking the median of all the individual pixel parameters (including nonenhancing pixels). The median rather than the mean was used because the distributions of the parameters were skewed. In muscle and kidney, tissue enhancement analysis was only done on a whole ROI basis. Two experienced observers working in consensus evaluated the patterns of enhancement within each tumor ROI by inspecting subtraction images obtained 90 seconds after injection and by reviewing transfer constant pixel maps (Fig 1). The patterns of enhancement changes at 4 and 24 hours after treatment were compared with the pretreatment patterns. The images were assessed for a visible reduction in enhancement within the center of tumors compared with that seen at the periphery.

*Data analysis.* When patients had two pretreatment DCE-MRI examinations, the mean value of each parameter was taken as the pretreatment value. The absolute difference and relative (percent) change in parameter values from this pretreatment value were calculated for all subsequent DCE-MRI examinations. In our reproducibility study,[21] we calculated the size of changes needed for statistical significance in individuals and in groups of patients. Two statistics from that study have been applied here: the repeatability or individual 95% limit of change gives the value of the absolute change in a parameter that might occur in an individual patient spontaneously. Any change greater than this value in an individual patient is considered to be statistically significant. The 95% limit of change for a group

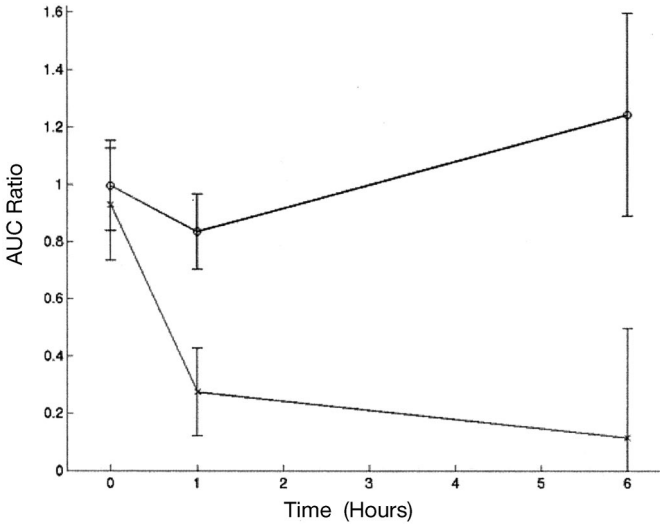


**Fig 2. Effect of saline (○) or combretastatin A4 phosphate 30 mg/kg (×) on area under the curve at 90 minutes ($AUC_{90}$) in (A) tumor, (B) kidney, and (C) muscle. Data are shown as mean ± SEM.**

of n patients can be determined from the value of the mean squared differences (dsd) derived from the reproducibility data set using the following formula:

$$\frac{1.96 \times \text{dsd}}{\sqrt{n}} \quad (4)$$

The dsd values for $\log_{10}K^{trans}$, $k_{ep}$, $v_e$, and AUC were 0.14 mL/mL/min, 0.40 mL/mL/min, 3.89 mL/mL%, and 0.05 M · min, respectively, for tumor and 0.31 mL/mL/min, 0.65 mL/mL/min, 2.97 mL/mL%, and 0.04 M · min, respectively, for muscle.[21] $K^{trans}$ values were logarithmically transformed because the variability in this parameter was dependent on the mean parameter value.[27] The mean difference in parameter values was compared with the 95% limit of change for groups established from these data. In addition, a paired Student's *t* test was performed to compare mean changes.

## RESULTS

### *Rat Studies*

The effects of CA4P or saline treatment on AUC values are shown in Figure 2 for tumor, muscle, and kidney. There was a large and statistically significant reduction in mean AUC at 1 and 6 hours in the tumor of 90% and 95%, respectively, after injection of CA4P 30 mg/kg compared with pretreatment values at these time points. Only minor recovery was observed at 24 hours and no reductions were seen in animals treated with saline. No significant changes were observed in muscle AUC. Although there was an indication of a reduction in kidney AUC at 6 hours after CA4P, this was not significant and a similar pattern was observed for the control group. The mean initial tumor $K^{trans}$ value was 0.17 mL/mL/min (standard deviation [SD], 0.11 mL/mL/min), and mean $v_e$ was 68 mL/mL% (SD, 60 mL/mL%). $K^{trans}$ was reduced by 73% and 64% at 1 and 6 hours, respectively, in tumor, with no significant changes in muscle (data not shown). $v_e$ was also reduced by 81% and 69% at 1 and 6 hours, respectively, in tumor. There were no significant changes in $k_{ep}$ values in tumor or muscle.

Figure 3 shows the effect of CA4P treatment on the ratio (central AUC):(peripheral AUC). Central AUC was calculated from pixels more than 5.0 mm from the tumor edge; peripheral AUC was calculated from pixels less than 2.0 mm from the edge. The initial ratio is approximately 1, but decreases significantly at 1 and 6 hours after CA4P injection ($P < .05$, paired *t* test) because of a larger vascular effect in the tumor center compared with that in the periphery. Nevertheless, significant decreases in AUC were observed in the tumor periphery (two- to four-fold), which compared with 10- to 20-fold AUC decreases in the center. No significant changes were seen in central tumor AUC, peripheral AUC, or their ratio for saline-treated animals (Fig 3).

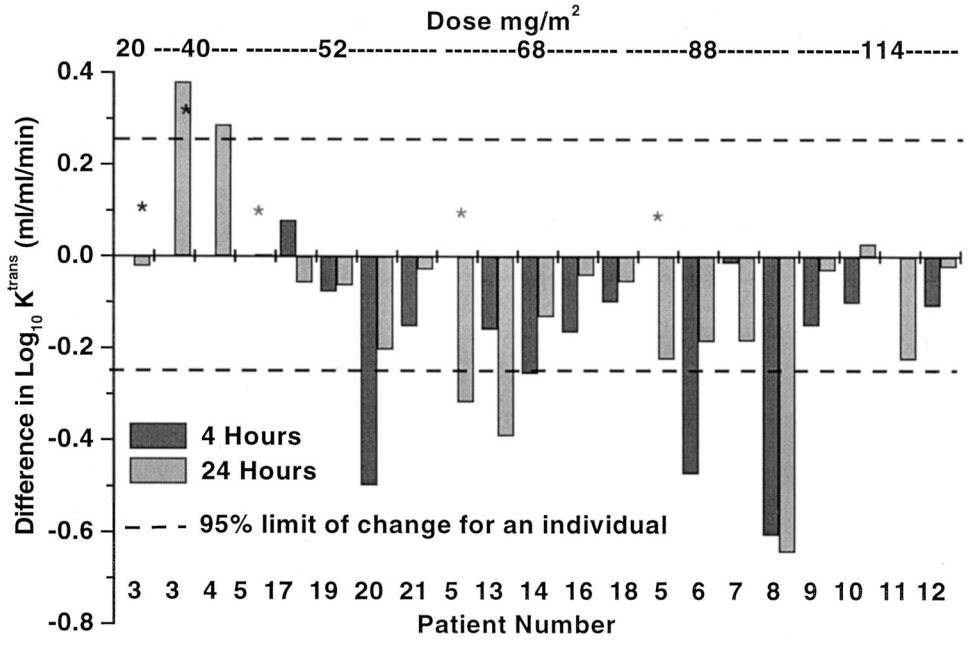


**Fig 3. Effect of saline (○) or combretastatin A4 phosphate 30 mg/kg (×) on tumor area under the curve at 90 seconds ($AUC_{90}$) shown as the ratio of central AUC:periphery AUC. Central pixels are more than 5.0 mm and peripheral pixels are less than 2.0 mm from the tumor edge. Data obtained from rats and shown as mean ± SEM.**

**Table 1. Patient Characteristics**

| Age (years) | Sex | Patient No. | Tumor Type | Tumor Site | Tumor Size (cm) |
|---|---|---|---|---|---|
| 50 | F | 1* | Ovarian serous cystadenocarcinoma | Pelvis | 13 × 11 |
| 64 | F | 2* | Ovarian serous cystadenocarcinoma | Pelvic mass | 7 × 7 |
| 45 | M | 3 | Non–small-cell lung cancer | Axilla | 5 × 4 |
| 59 | F | 4 | Renal spindle cell carcinoma | Renal bed | 13.5 × 10.5 |
| 61 | M | 5 | Melanoma | Groin node | 9 × 6.5 |
| 58 | F | 6 | Leiomyosarcoma | Para-aortic lymph node | 8 × 8 |
| 69 | F | 7 | Ovarian serous cystadenocarcinoma | Para-aortic node | 9 × 6 |
| 62 | F | 8 | Leiomyosarcoma | Chest | 19 × 17 |
| 57 | F | 9 | Ovarian serous cystadenocarcinoma | Inguinal lymph node | 6 × 5.5 |
| 44 | F | 10 | Renal cell carcinoma | Renal bed | 5 × 5 |
| 60 | F | 11 | Renal cell carcinoma | Kidney | 13 × 13 |
| 41 | M | 12 | Renal cell carcinoma | Para-aortic node | 4.5 × 3 |
| 47 | F | 13 | Adrenocortical carcinoma | Liver | 5 × 3.5 |
| 55 | F | 14 | Colonic adenocarcinoma | Spleen | 8 × 5 |
| 40 | F | 15* | Peritoneal carcinoma | Pelvis | 6.5 × 5.5 |
| 46 | F | 16 | Breast adenocarcinoma | Pelvis | 9 × 7 |
| 63 | F | 17 | Leiomyosarcoma | Pelvis | 17 × 9 |
| 48 | M | 18 | Leiomyosarcoma | Chest | 18 × 16 |
| 69 | F | 19 | Leiomyosarcoma | Pelvis | 17 × 14 |
| 57 | F | 20 | Peritoneal carcinoma | Pelvis | 3 × 2 |
| 62 | M | 21 | Spindle cell sarcoma | Suprarenal mass | 15 × 13 |

Abbreviations: M, male; F, female.
*Patient excluded from final analysis.

*Clinical Studies*

*Treatment received.* Twenty-one patients underwent DCE-MRI examinations and were treated at CA4P doses from 5 to 114 mg/m$^2$. The data for the first two patients were rejected for technical reasons (poor signal-to-noise ratio). The subsequent 19 patients were examined using the DCE-MRI protocol described above. Table 1 lists the patient characteristics. The range of tumor types is typical for patients in phase I clinical trials, although most of the tumors were large. Eleven of these patients form part of the reproducibility data set described in our previous study.[21] One patient had DCE-MRI examinations at 20 and 40 mg/m$^2$ dose levels, and another patient had examinations at 52, 68, and 88 mg/m$^2$ dose levels. The remaining 17 patients had DCE-MRI examinations at one dose level only. Of these, five patients had a second cycle of three infusions and one patient had a series of eight cycles (24 infusions). One patient (patient 15) treated at 52 mg/m$^2$ was subsequently excluded. She had an ovarian carcinoma with abdominal ascites. This required drainage between the pretreatment examinations and twice during the first cycle of treatment. The accumulation and drainage of fluid caused changes in the appearance of the tumor such that adequate registration of posttreatment images with pretreatment images was impossible. Thus, 18 patients had DCE-MRI data that were used for the final analysis.

*Toxicities*

Toxicities seen in this trial are fully reported in the accompanying article[8] and 68 mg/m$^2$ was established as the maximum-tolerated dose (MTD). Changes in vital signs were seen after CA4P treatment.[8] There were no significant changes in the group treated at 5 to 40 mg/m$^2$. At 52 to 114 mg/m$^2$, blood pressure was significantly increased by a mean of 11 mmHg systolic (8%) and 8 mmHg diastolic (10%) 30 minutes to 1 hour after treatment, and was associated with a 15% decrease in heart rate. Four hours after treatment systolic and diastolic blood pressure were significantly decreased compared with baseline by a mean of 8 and 6 mmHg (6% and 7%), respectively, and heart rate was increased by 15% to 98 beats/min. After 24 hours there was no significant difference in heart rate (84 beats/min) or blood pressure (132/78 mmHg) compared with baseline measurements (85 beats/min and 132/80 mmHg).

*DCE-MRI Results: Tumor*

The mean initial tumor $K^{trans}$ value was 0.68 mL/mL/min (SD, 0.64 mL/mL/min) and mean $v_e$ was 31.8 mL/mL% (SD, 14.2 mL/mL%). These values are comparable with those in the literature for human tumors.[28,29] The absolute change in each parameter, 4 hours and 24 hours after the first dose of CA4P, is shown in Figure 4, which shows evidence of a dose effect. No significant change in $\log_{10}K^{trans}$ is seen in those patients treated at doses up to 40 mg/m$^2$, but six of 16 patients treated at $\geq$ 52 mg/m$^2$ had significant reductions in $\log_{10}K^{trans}$ at either 4 or 24 hours, and several others had reductions that did not quite reach significance. The relative reduction in $K^{trans}$ ranged from 44% to 77% in these six patients. Additional evidence for this dose effect is given by a significant correlation ($R = 0.48$; $P = .03$) between the concentration of CA4 AUC derived from plasma pharmacokinetic studies with maximum relative reduction in $K^{trans}$ after the first dose of CA4P (Fig 5).

Most patients had the greatest reduction of $\log_{10}K^{trans}$ at 4 hours, with just one patient having a significant reduction only at 24 hours. At the DCE-MRI examinations 24 hours after the first dose or 13 days after the last dose of CA4P, five of eight patients treated at $\geq$ 88 mg/m$^2$ had significant decreases in $v_e$ greater than

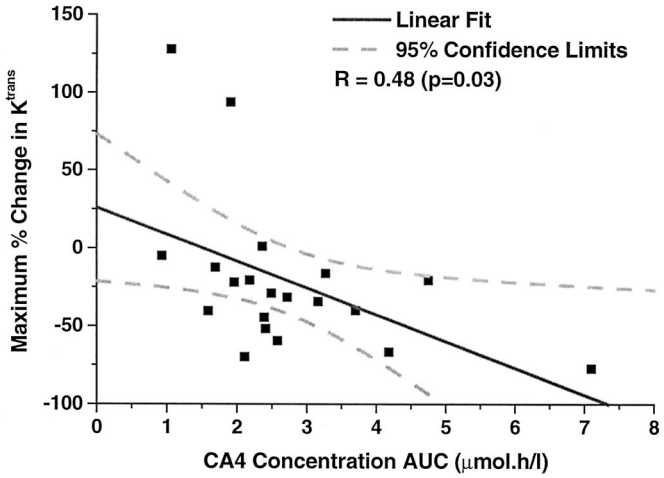


**Fig 4. Absolute change in tumor $\log_{10} K^{trans}$ 4 and 24 hours after the first dose of combretastatin A4 phosphate for patients in the phase I trial. (*) Patients treated at more than one dose level. The 95% limit of change is explained in Data Analysis.**

6.9 mL/mL%. Of these, four patients had an associated increase in the number of completely nonenhancing pixels (Table 2). This is illustrated in Figure 1, in which parameter maps for $K^{trans}$ before treatment and at several points after treatment for a patient (patient 6) treated at 88 mg/m$^2$ are shown. The heterogeneity within the tumor is seen on the pretreatment map. After treatment there is a marked reduction in $K^{trans}$ values, particularly in the center of the tumor, with some sparing of the tumor rim. This pattern is similar to the pattern of post-CA4P changes observed in the rat tumors (Fig 3). The patient whose data are shown in Fig 1 had a total of six doses of CA4P. There was a marked increase in nonenhancing (black) pixels within the tumor ROI after treatment from 20% pretreatment to 64% 13 days after the last dose of CA4P. A reduction in $K^{trans}$ levels was visible on the parameter maps in 14 of 18 patients at either the 4- or 24-hour time points. In six of these 14 patients (patients 5, 6, 8, 9, 11, and 20), a greater reduction in the center than at the edge of marker lesions was seen (marked central reduction in four patients), as illustrated in Figure 1.

Because there was no evidence of consistent reductions in DCE-MRI parameters at 20 to 40 mg/m$^2$, mean changes after treatment were calculated for all 16 patients treated at or above 52 mg/m$^2$. Because 68 mg/m$^2$ was established as the MTD,[8] mean reductions were also calculated in the nine patients treated in the well-tolerated dose range of 52 to 68 mg/m$^2$ who had DCE-MRI examinations. Mean $\log_{10} K^{trans}$ was reduced by 0.20 mL/mL/min (37%) at 4 hours ($P = .002$, paired $t$ test) and by 0.15 (29%) at 24 hours after the first dose ($P = .003$). Both of these reductions were greater than the 95% limits of change determined from the reproducibility data set (0.068 and 0.064 mL/mL/min calculated for a group of 14 and 16 patients,

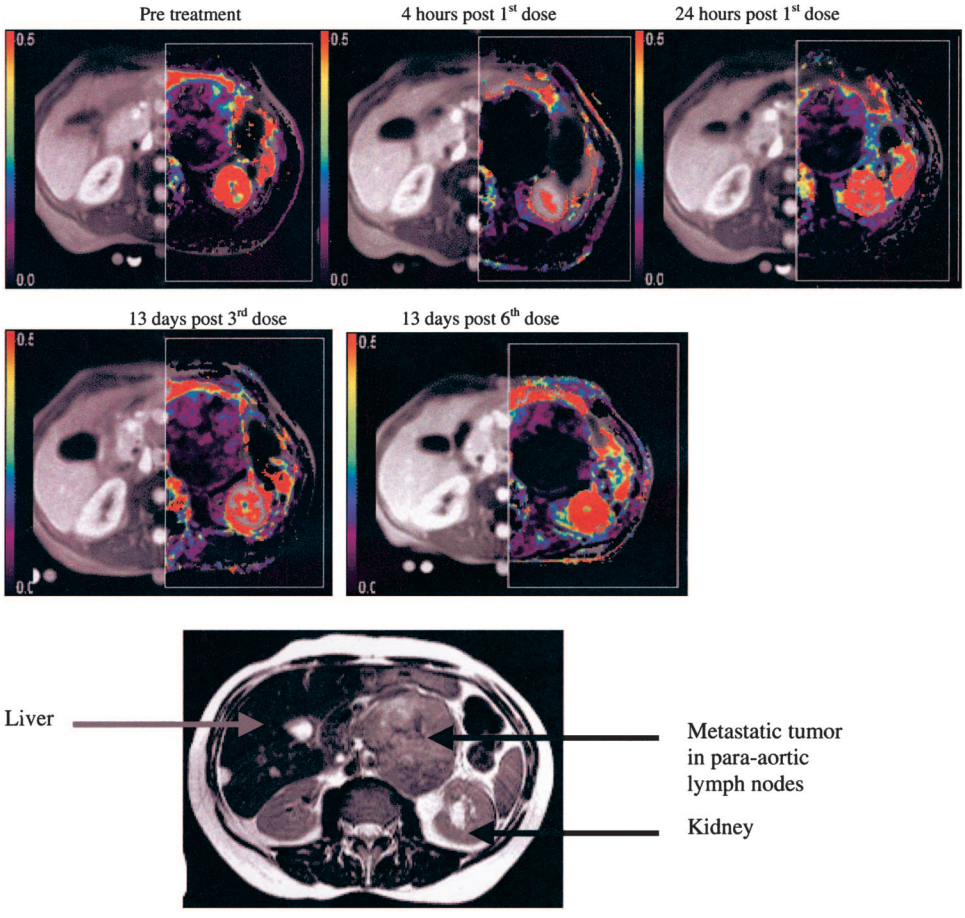


**Fig 5. Linear regression plot of maximum change in $K^{trans}$ versus exposure of the active combretastatin A4 (CA4; area under the concentration-time curve [AUC] of CA4).**

**Table 2. Dynamic Contrast Enhanced Magnetic Resonance Imaging Parameters in Tumor Regions of Interest at Baseline and Change in Parameters at 4 and 24 Hours After the First Dose of CA4P**

| | | Baseline Values: Tumor | | | | 4 Hours After CA4P: Tumor | | | | 24 Hours After CA4P: Tumor | | | |
|---|---|---|---|---|---|---|---|---|---|---|---|---|---|
| Patient No. | CA4P Dose ($mg/m^2$) | % Nonenhancing Pixels | Transfer Constant (mL/mL/min) | Leakage Space (mL/mL %) | AUC (M · min) | % Nonenhancing Pixels Change | Transfer Constant Change (%) | Leakage Space Change (%) | AUC Change (%) | % Nonenhancing Pixels Change | Transfer Constant Change (%) | Leakage Space Change (%) | AUC Change (%) |
| 3 | 20 | 0 | 0.61 | 36 | 0.30 | | | | | 0 | −5 | −24 | −20 |
| 3 | 40 | 0 | 0.54 | 31 | 0.22 | | | | | 0 | 140 | 4 | 41 |
| 4 | 40 | 23 | 0.17 | 10 | 0.07 | | | | | −11 | 94 | 26 | 47 |
| 5 | 52 | 17 | 0.18 | 8 | 0.07 | | | | | −1 | 1 | 34 | 20 |
| 17 | 52 | 1 | 0.88 | 48 | 0.40 | −1 | 20 | 7 | 2 | −1 | −12 | −4 | −4 |
| 19 | 52 | 0 | 0.42 | 31 | 0.22 | 0 | −16 | −4 | −23 | 0 | −13 | −7 | −20 |
| 20 | 52 | 0 | 0.43 | 35 | 0.25 | 1 | −68 | −33 | −59 | 0 | −37 | −10 | −20 |
| 21 | 52 | 13 | 0.65 | 44 | 0.34 | −5 | −30 | 7 | −12 | −5 | −6 | 5 | −9 |
| 5 | 68 | 24 | 0.31 | 9 | 0.08 | | | | | −8 | −52 | −11 | −18 |
| 13 | 68 | 0 | 2.34 | 58 | 0.66 | 0 | −31 | −21 | −19 | 0 | −59 | −8 | −22 |
| 14 | 68 | 0 | 2.16 | 50 | 0.60 | 0 | −44 | −43 | −59 | 0 | −26 | −2 | −10 |
| 16 | 68 | 1 | 0.42 | 39 | 0.25 | +6 | −32 | −15 | −27 | +6 | −9 | −9 | −16 |
| 18 | 68 | 2 | 0.35 | 26 | 0.20 | 0 | −20 | −12 | −17 | +1 | −12 | −9 | −16 |
| 5 | 88 | 27 | 0.33 | 7 | 0.07 | | | | | −5 | −40 | 27 | −16 |
| 6 | 88 | 20 | 0.10 | 16 | 0.07 | +68 | −66 | −8 | −72 | +7 | −35 | −11 | −33 |
| 7 | 88 | 0 | 0.29 | 19 | 0.13 | +1 | −3 | −19 | −7 | +18 | −34 | −15 | −15 |
| 8 | 88 | 8 | 0.98 | 40 | 0.35 | +10 | −75 | −41 | −56 | +30 | −77 | −69 | −72 |
| 9 | 114 | 2 | 0.21 | 35 | 0.13 | −2 | −29 | −40 | −26 | −2 | −7 | −29 | −12 |
| 10 | 114 | 0 | 1.13 | 34 | 0.34 | 0 | −21 | −34 | −32 | 0 | 7 | −14 | −15 |
| 11 | 114 | 45 | 0.15 | 12 | 0.08 | | | | | +12 | −40 | −27 | −38 |
| 12 | 114 | 0 | 0.68 | 34 | 0.29 | 0 | −22 | −5 | −13 | 0 | −5 | 17 | 1 |

Abbreviations: CA4P, combretastatin A4 phosphate; AUC, area under the curve.

respectively). $v_e$ was also significantly reduced at 4 and 24 hours; values were 7.0 mL/mL% (21%) at 4 hours ($P = .005$) and 3.7 mL/mL% (11%) at 24 hours ($P = .03$), but at the end of the cycle there was no significant difference from pretreatment. These reductions are also greater than the 95% limits of change (1.85 and 1.73 mL/mL% for groups of 14 and 16 patients, respectively). The mean reduction in $\log_{10}K^{trans}$ and $v_e$ in tumor ROIs for all patients treated at $\geq 52$ mg/m$^2$ 4 hours and 24 hours after the first dose of CA4P, and 13 days after the third dose are shown in Figure 6.

If the patients treated at dose levels above the MTD are excluded from this analysis (leaving the nine patients treated at 52 and 68 mg/m$^2$), the mean reduction in $\log_{10}K^{trans}$ was 0.17 (32%; $P = .03$) and 0.13 mL/mL/min (25%; $P = .01$) at 4 and 24 hours, respectively. These reductions are still greater than the 95% limits of change (0.090 and 0.085 for groups of eight and nine patients, respectively). The mean reduction in $v_e$ for this group was 6.1 mL/mL% (16%; $P = .04$) and 1.8 mL/mL% (5%; $P = .02$) at 4 and 24 hours, respectively (95% limits were 2.45 and 2.31 mL/mL%, respectively). Tumor AUC followed a similar pattern as that described for $K^{trans}$, with six patients having significant reductions at 4 or 24 hours. There was a significant mean reduction in patients treated at $\geq 52$ mg/m$^2$ of 33% ($P = .004$) and 18% ($P = .006$) at 4 and 24 hours, respectively. These reductions are also greater than the 95% limits of change (13% and 12% for groups of 14 and 16 patients, respectively).

### *DCE-MRI Results: Normal Tissues*

In contrast to the changes seen in tumors, the changes in parameters seen in muscle appeared to be random. There were no significant group changes observed at any time point (Fig 6). One patient (patient 14) treated at 68 mg/m$^2$ had a significant reduction in kidney AUC of 53% at 24 hours, which had recovered by the next DCE-MRI examination 13 days after the third dose of CA4P, and was not associated with symptoms or with an increase in serum urea or creatinine. There was no significant mean reduction in kidney AUC at any time point; the AUC at 4 and 24 hours was reduced by 2% and 0.5%, respectively, compared with the pretreatment value.

## DISCUSSION

The effects of CA4P on the vasculature of tumors in mice and rats have been demonstrated by the use of radioactive tracer uptake methods,[5-7] histologic assessment of functional vascular volume,[5] and the noninvasive technique DCE-MRI.[17,19,30-32] In particular, Prise et al[7] showed 87% and 98% reductions in blood flow for the P22 tumor 1 and 6 hours, respectively, after administration of 30 mg/kg CA4P. Changes observed in this study for P22 tumors in DCE-MRI parameters, especially Gd-DTPA AUC (95% reduction at 6 hours) and, to a lesser extent $K^{trans}$ and $v_e$, were comparable to those observed in our study. The plasma exposure to the active agent (CA4) in rats at this dose level was 12.8 $\mu$mol h L$^{-1}$ (AUC[7]) which is higher than the range seen in patients.[8] However, even at 10 mg/kg (corresponding to a CA4 exposure of 3.76 $\mu$mol h L$^{-1}$), Prise et al observed a substantial blood flow reduction (92% at 6 hours) and histologic changes including hemorrhage and the development of moderate central necrosis.

To interpret the results of DCE-MRI studies, it is helpful to consider the physiologic parameters, which determine the behavior in tissues of low molecular weight contrast media such as

**Table 3. Dynamic Contrast Enhanced Magnetic Resonance Imaging Parameters in Muscle and Kidney Regions of Interest at Baseline and Change in Parameters at 4 and 24 Hours After the First Dose of CA4P**

| | | Baseline Values: Muscle | | 4 Hours After CA4P: Muscle | | 24 Hours After CA4P: Muscle | | | | |
|---|---|---|---|---|---|---|---|---|---|---|
| Patient No. | CA4P Dose ($mg/m^2$) | Transfer Constant (mL/mL/min) | Leakage Space (mL/mL %) | Transfer Constant Change (%) | Leakage Space Change (%) | Transfer Constant Change (%) | Leakage Space Change (%) | Baseline AUC Values: Kidney (%) | AUC 4 Hours After CA4P: Kidney (%) | AUC Change 24 Hours After CA4P: Kidney (%) |
| 3 | 20 | 0.07 | 8 | | | −50 | −21 | | | |
| 3 | 40 | 0.04 | 10 | | | 76 | −22 | | | |
| 4 | 40 | 0.03 | 10 | | | | | | | |
| 5 | 52 | 0.17 | 7 | | | 6 | 3 | | | |
| 17 | 52 | 0.28 | 20 | −17 | −30.20 | −59 | −36 | 0.572 | 14.2 | 14.5 |
| 19 | 52 | 0.30 | 13 | 260 | 67.44 | 532 | 69 | 0.532 | 40.7 | 6.5 |
| 20 | 52 | 0.20 | 21 | 8 | 41.23 | −27 | 15 | 0.806 | 27.6 | 24.4 |
| 21 | 52 | 0.08 | 17 | 35 | −35.26 | 103 | −38 | 0.604 | −5.8 | 7.4 |
| 5 | 52 | 0.17 | 7 | | | 6 | 3 | | | |
| 17 | 52 | 0.28 | 20 | −17 | −30.20 | −59 | −36 | 0.572 | 14.2 | 14.5 |
| 19 | 52 | 0.30 | 13 | 260 | 67.44 | 532 | 69 | 0.532 | 40.7 | 6.5 |
| 20 | 52 | 0.20 | 21 | 8 | 41.23 | −27 | 15 | 0.806 | 27.6 | 24.4 |
| 21 | 52 | 0.08 | 17 | 35 | −35.26 | 103 | −38 | 0.604 | −5.8 | 7.4 |
| 5 | 68 | 0.11 | 6 | | | 64 | 8 | | | |
| 13 | 68 | 0.07 | 10 | 20 | −13.91 | 9 | 17 | 0.676 | −3.7 | 2.5 |
| 14 | 68 | 0.18 | 14 | −37 | −9.49 | 111 | −8 | 0.615 | −22.3 | −52.7 |
| 16 | 68 | 0.60 | 17 | 40 | −18.13 | −35 | −11 | 0.550 | −26.2 | −5.4 |
| 18 | 68 | 0.12 | 10 | −19 | −12.50 | 32 | 105 | 0.671 | −23.0 | −3.8 |
| 5 | 88 | 0.14 | 7 | | | −26 | −2 | | | |
| 6 | 88 | 0.05 | 4 | −41 | 1.09 | −29 | 66 | 0.610 | 10.6 | 34.3 |
| 7 | 88 | 0.08 | 8 | −40 | −20.02 | −51 | 11 | | | |
| 8 | 88 | 0.14 | 9 | −57 | 13.59 | −66 | −52 | 0.442 | −11.2 | −19.9 |
| 9 | 114 | 0.04 | 20 | 125 | −26.59 | −34 | 67 | 1.046 | 8.7 | 11.7 |
| 10 | 114 | 0.07 | 11 | −68 | −83.36 | 9 | −8 | 0.447 | −35.9 | −18.6 |
| 11 | 114 | 0.07 | 11 | | | 9 | −9 | 0.581 | −2.3 | −11.2 |
| 12 | 114 | 0.10 | 11 | −41 | 2.18 | −28 | −11 | 0.688 | −15.5 | −17.8 |

Abbreviations: CA4P, combretastatin A4 phosphate; AUC, area under the curve.

Gd-DTPA. In a tissue with highly permeable blood vessels, the rate at which Gd-DTPA enters the EES is limited by the tissue blood flow rate rather than extravasation rate, and in this situation the parameter $K^{trans}$ is equivalent to the blood plasma flow per unit volume of tissue.[11] In a tissue such as brain with a tight blood-brain barrier, the rate at which Gd-DTPA enters the EES is limited by its extravasation rate, and in this situation, $K^{trans}$ is equivalent to the product of the permeability and surface area. In tumors, vessels are generally more permeable than normal tissues, but the permeability is heterogeneous across the tumor. Whole tumor ROI estimates of $K^{trans}$ will therefore reflect a combination of vascular permeability, vessel surface area, and perfusion. In necrotic regions with a poor blood supply, low $K^{trans}$ values may be observed despite high vessel permeability.[33] Therefore, nonenhancing pixels were considered to represent areas of necrosis. It should also be noted that the decrease in $v_e$ for both human and rat tumors is not consistent with the expected changes in EES after CA4P treatment because an increase in this physical space may be expected as a result of edema or necrosis (or both). It may be better to describe $v_e$ as the EES of the well-perfused tumor fraction. The pretreatment values of $v_e$ in rat tumors are also unexpectedly high, but this could be the result of uncertainties in scaling between rat tissue Gd-DTPA concentrations and the assumed rat AIF.

There are uncertainties in the accuracy of kinetic parameter estimates derived from the application of tracer kinetic models in clinical DCE-MRI experiments. These derive from model-based assumptions and from assumptions made for the determination of tissue Gd-DTPA concentrations. For the Tofts' model used in this study, a standard AIF was used,[26] and it is assumed that the supply of contrast medium is not perfusion limited and that tissue blood volume contributes negligible signal compared with that arising from contrast medium in the interstitial space.[34] Buckley suggested that the application of commonly accepted models and their respective model-based assumptions to DCE-MRI data leads to systematic overestimation of the transfer constant in tumors.[35] It is also important to note that in DCE-MRI experiments, the contrast medium is detected only indirectly by its effect on the water signal. In tissues, contrast media are confined to the extracellular space, whereas the bulk of the water is intracellular. As a result, transmembrane water exchange can affect the accuracy of the tissue contrast agent concentration estimate.[36,37]

Another important factor in determining the contrast agent concentration is extracellular macromolecular content.[38] The experimental conditions that we used in the dynamic component of the examinations should minimize these effects, and our estimate of error in ignoring transmembrane water exchange is likely to be small (probably $< 10\%$). As a result, it is difficult to be certain about how accurately model-based kinetic parameter estimates compare with the physiologic parameter that they purport to measure. This is a difficult factor to determine

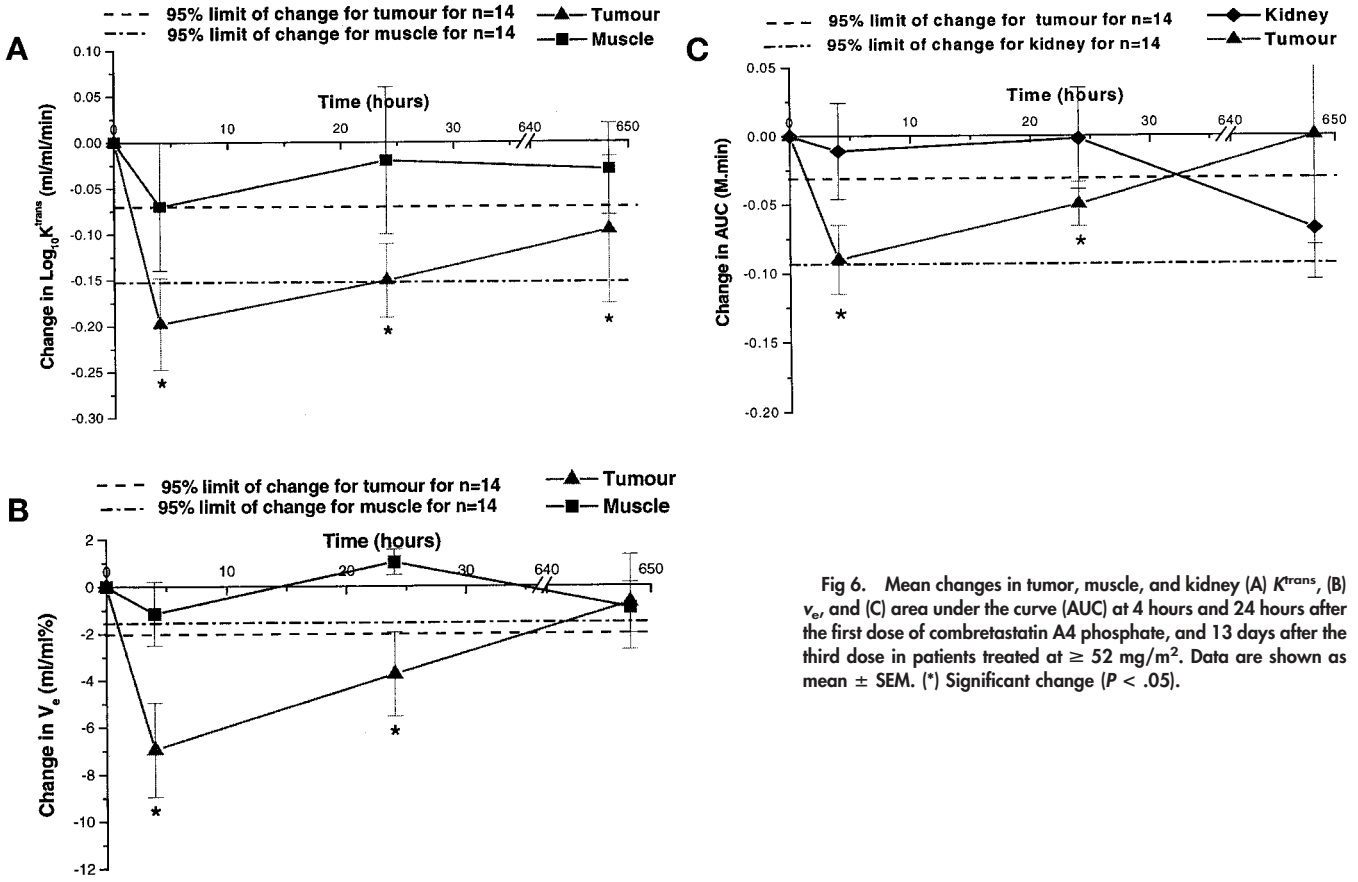


**Fig 6.** Mean changes in tumor, muscle, and kidney (A) $K^{trans}$, (B) $v_e$, and (C) area under the curve (AUC) at 4 hours and 24 hours after the first dose of combretastatin A4 phosphate, and 13 days after the third dose in patients treated at ≥ 52 mg/m$^2$. Data are shown as mean ± SEM. (*) Significant change ($P < .05$).

accurately because of the lack of a reliable clinical gold standard. In addition, because the slice positioning from visit to visit will not be identical, despite the rigorous efforts made there is a potential for errors caused by positional artifacts. An additional limitation is the use of a generalized rather than individual AIF. As Rijpkema et al[39] have shown, the use of a generalized AIF significantly affects reproducibility. If the data they reported for $k_{ep}$ in 11 patients are used to calculate 95% limits of change, these limits increase from 11% with individual AIFs to 19% using a generalized AIF. A 50% change in the peak value of the AIF produced a 10% change in the $k_{ep}$ value. Despite these limitations, in the context of this study, changes in $K^{trans}$ (as opposed to absolute values) are likely to be meaningful for two reasons.

First, we have established the reproducibility of the technique.[21] The mean 37% reduction in $K^{trans}$ seen in patients treated at 52 mg/m$^2$ and higher in this study was considerably greater than the 95% limit of change (14% reduction) established in the same study. This limit includes errors caused by the use of a generalized rather than individual AIF. The potential repositioning errors are also applicable to that study, and the 95% limits include such errors. Significant reductions in $v_e$ and increases in numbers of nonenhancing pixels within tumors indicate local vascular shutdown within the tissue as the mechanism of action, rather than global reduction in blood flow.

Second, we previously showed that the pattern of reduction of blood flow measured by IAP in a rat carcinosarcoma model after administration of CA4P is similar in time course and extent to the reduction in kinetic parameters measured by DCE-MRI in the same model system.[17] This animal study was designed as a follow-up to the initial work and, in contrast to that work, used serial imaging of individual animals to parallel the clinical study.

Furthermore, if one accepts that there are outstanding issues with regard to model-based assumptions and the measurement of tissue contrast agent concentration, quantitative techniques such as those used in this study do enable a comparison of data acquired serially in patients and in different patients examined at the same or different scanning sites; these assumptions indicate an important, practical drug development and evaluation issue. Although a reduction in the semiquantitative parameter gradient was seen in six of seven patients at 60 mg/m$^2$ in another phase I trial of CA4P,[40] the extent of reduction is difficult to relate to preclinical models and to data from other sites because the change in signal intensity seen is dependent on the initial tissue T1 value as well as on machine and scaling factors.

The changes in $K^{trans}$ and AUC seen in patients treated in this phase I trial of CA4P therefore demonstrate that CA4P has antivascular activity in tumors at doses at and below the dose-limiting toxicity. No significant changes were seen in the patients treated at 20 and 40 mg/m$^2$, which indicates that there may be a threshold dose level below which effects on the microvasculature are not seen. If we consider the group of patients treated at 52 mg/m$^2$ and above as a whole, the time course of the changes is similar to that seen in rats; that is, the

effect at 4 hours tended to be greater than that seen at 24 hours. However, the opposite was found for a few individuals after the first dose. This may reflect differences in tumor vasculature because CA4 has a short half-life, with more than 95% cleared in the first 4 hours,[8] so the changes seen at 24 hours do not reflect continuing drug exposure, but continuing consequences of events initiated by drug exposure. Indeed there was no corresponding prolongation of the clearance of CA4 from the plasma in those patients with significant DCE-MRI changes at 24 hours (data not shown). A more prolonged reduction in blood flow might be expected to cause increased tumor cell death, although reperfusion injuries after shorter duration ischemia[41] and neutrophil infiltration[42] also influence tumor-cell kill. This cohort of patients is too small to correlate temporal pattern of blood flow response with clinical effect, although the patient (patient 13) who had a 50% reduction in tumor size after 12 doses of CA4P had a greater reduction in tumor $K^{trans}$ at 24 hours than at 4 hours.

The DCE-MRI data in both rats and human patients indicate that at 4 to 6 hours after administration of CA4P there is a relatively selective effect on tumor, with no significant reduction in mean kinetic parameters in muscle or kidney. Perfusion PET imaging was performed in this trial 30 minutes after administration of CA4P and there was a mean reduction in spleen blood flow of 35%, but no significant change in kidney blood flow.[9] A significant mean reduction in cardiac output of 9% was seen at 30 minutes after treatment with CA4P in the PET study, which coincided with the peak increase in blood pressure and decrease in heart rate. At the time of the 4-hour MRI examination, blood pressure was reduced and heart rate increased. The effects on cardiac output at the examination times in the PET and DCE-MRI studies may therefore be different. Indeed, there was no reduction in stroke volume seen in the PET study, indicating that the observed changes in heart rate were reflected in the cardiac output changes. The changes observed in blood pressure and heart rate follow a similar pattern to those seen in rats bearing P22 carcinosarcomas, although the percentage increase in blood pressure was greater[7] in rats at 1 hour than in humans 30 minutes after treatment. As in humans, hypertension in the rat was associated with a relative bradycardia. By 6 hours after treatment, blood pressure in the rat had returned to baseline but heart rate was increased, as seen in the clinical studies.

The change in tumor blood flow after administration of CA4P is greater than that seen with drugs affecting systemic hemodynamics. Limited changes in tumor blood flow in rats have been seen with hypertensive agents such as angiotensin II,[18] but only at doses that caused much larger changes in blood pressure and heart rate than observed in either this study or after CA4P treatment in rats.[6] Larger reductions were seen in normal tissue blood flow. Other studies have shown an increase in tumor blood flow with angiotensin II relative to that in normal tissues.[43,44] Reduced tumor blood flow has also been observed in experimental models after treatment with higher doses of the vasodilator hydralazine,[45,46] which also reduced blood pressure by 50%. The changes in blood pressure seen in this study are therefore much smaller than those needed to produce significant reductions in tumor blood flow in the above-described studies. This indicates that the changes seen in patients treated with CA4P are due to a direct effect on local tumor vasculature rather than solely to a systemic effect such as a change in blood pressure or cardiac output. The blood pressure and cardiac output changes are more likely to be a reflection of increased vascular resistance to a variable degree in a range of tissues including tumors.

CA4 depolymerizes microtubules and this leads to a rapid and marked shape change in proliferating human endothelial cells.[47,48] The time course of the endothelial cell shape change and a corresponding increase in endothelial cell monolayer permeability[49] are similar to that for the reduction in tumor blood flow,[48] and also for an early increase in tumor vascular permeability in vivo.[50] Thus, CA4P may produce an additional increase in the abnormally high interstitial fluid pressure in tumors,[51-53] and thereby lead to vascular collapse.[54,55] The combination of proliferating endothelium and increased interstitial fluid pressure in tumors may explain some of the tumor selectivity shown by CA4P. However, as discussed above, changes in blood flow have also been observed in some normal tissues, and these observations raise questions about the precise mechanism of action of CA4P. Although greater shape change effects were seen in proliferating cells, at the concentrations achieved in plasma in patients, some effects were seen in quiescent confluent endothelial cells.[21,50] These may be sufficient to cause increased vascular permeability in normal tissues. Endothelial cells also have major roles in the secretion of local vasoconstricting and vasodilating agents such as endothelin and nitric oxide. Microtubules are involved in the intracellular positioning and transport of organelles, which may be important in the secretion of these agents.[56-59] Disruption of this network is therefore likely to have effects on the balance of vasoconstricting versus dilating factors, and may have different effects in different tissues. Additional studies are required to investigate these hypotheses further.

The clear difference between the response to CA4P of central and peripheral regions of the P22 rat tumor detected here is compatible with relative (but not absolute) sparing of blood vessels near the tumor edge. Peripheral sparing has not always been observed in animal models and was not found in our previous MRI study of the P22 tumor.[17] This possibly was because of the use of a surface coil (which had a heterogeneous response throughout the tumor slice) or the lack of repeat measurements in individual tumors in that study design. Likewise, the evidence for this phenomenon from IAP uptake measurement of blood flow in the P22 tumor is ambiguous.[6,7] Visual inspection of parametric images, which demonstrate the heterogeneity of change in $K^{trans}$ and $v_e$ across the tumors in patients, provides preliminary evidence for selectivity of CA4P for the tumor center in some but not all human tumors. Additional studies are required to clarify the relationship between tumor blood flow changes and the clear sparing of the tumor periphery, in terms of necrosis induction, which occurs even after the most effective doses of CA4P in animal models.[5]

In conclusion, we have shown that treatment with CA4P at well-tolerated doses produces significant reductions in human tu-

mor $K^{trans}$ and other DCE-MRI parameters, which are greater than those expected spontaneously, with no significant mean change in muscle or kidney. The time course of changes in rat and human tumors was similar, which demonstrates the utility of this animal model for preclinical studies of tumor vascular targeting agents. In humans, there was some recovery by 24 hours in most patients, which is consistent with published data for animals at equivalent exposures. These data demonstrate proof of principle that CA4P has tumor antivascular activity in humans, and provide support for additional clinical development of this agent, particularly in combination with conventional anticancer therapies.

## REFERENCES


1. Pettit GR, Cragg GM, Herald DL, et al: Isolation and structure of combretastatin. Can J Chem 60:1374-1376, 1982
2. Hamel E, Lin CM: Interactions of combretastatin, a new plant-derived anti-mitotic agent, with tubulin. Biochem Pharmacol 32:3864-3867, 1983
3. Pettit GR, Singh SB, Hamel E, et al: Isolation and structure of the strong growth and tubulin inhibitor combretastatin A-4. Experentia 45:209-211, 1989
4. Pettit GR, Temple C Jr, Narayanan VL, et al: Antineoplastic agents 322. synthesis of combretastatin A-4 prodrugs. Anticancer Drug Des 10:299-309, 1995
5. Dark GG, Hill SA, Prise VE, et al: Combretastatin A-4, an agent that displays potent and selective toxicity toward tumor vasculature. Cancer Res 57:1829-1834, 1997
6. Tozer GM, Prise VE, Wilson J, et al: Combretastatin A-4 phosphate as a tumor vascular-targeting agent: Early effects in tumors and normal tissues. Cancer Res 59:1626-1634, 1999
7. Prise VE, Honess DJ, Stratford MR, et al: The vascular response of tumor and normal tissues in the rat to the vascular targeting agent, combretastatin A-4-phosphate, at clinically relevant doses. Int J Oncol 21:717-726, 2002
8. Rustin GJS, Galbraith SM, Anderson H, et al: Phase I clinical trial of weekly combretastatin A4 phosphate (CA4P): Clinical and pharmacokinetic results. J Clin Oncol 21:2815-2822, 2003
9. Anderson HL, Yap JT, Miller MP, et al: Assessment of pharmacodynamic vascular response in a phase I trial of combretastatin A4 phosphate. J Clin Oncol 21:2823-2830, 2003
10. Padhani AR: Dynamic contrast-enhanced MRI in clinical oncology: Current status and future directions. J Magn Reson Imaging 16:407-422, 2002
11. Tofts P, Brix G, Buckley D, et al: Estimating kinetic parameters from dynamic contrast-enhanced T(1)-weighted MRI of a diffusable tracer: Standardized quantities and symbols. J Magn Reson Imaging 10:223-232, 1999
12. Barentsz JO, Berger-Hartog O, Witjes JA, et al: Evaluation of chemotherapy in advanced urinary bladder cancer with fast dynamic contrast-enhanced MR imaging. Radiology 207:791-797, 1998
13. Mayr NA, Hawighorst H, Yuh WT, et al: MR microcirculation assessment in cervical cancer: Correlations with histomorphological tumor markers and clinical outcome. J Magn Reson Imaging 10:267-276, 1999
14. Reddick W, Bhargava R, Taylor J, et al: Dynamic contrast-enhanced MR imaging evaluation of osteosarcoma response to neoadjuvant chemotherapy. J Magn Reson Imaging 5:689-694, 1995
15. Padhani AR, MacVicar AD, Gapinski CJ, et al: Effects of androgen deprivation on prostatic morphology and vascular permeability evaluated with MR imaging. Radiology 218:365-374, 2001
16. Hawighorst H, Engenhart R, Knopp MV, et al: Intracranial meningiomas: Time- and dose-dependent effects of irradiation on tumor microcirculation monitored by dynamic MR imaging. Magn Reson Imaging 15:423-432, 1997
17. Maxwell RJ, Wilson J, Prise VE, et al: Evaluation of the anti-vascular effects of combretastatin in rodent tumors by dynamic contrast enhanced MRI. NMR Biomed 15:89-98, 2002
18. Tozer GM, Shaffi KM: Modification of tumor blood flow using the hypertensive agent, angiotensin II. Br J Cancer 67:981-988, 1993
19. Maxwell R, Wilson J, Tozer G, et al: Segmentation of magnetic resonance images according to contrast agent uptake kinetics using a comparative neural network, in Malmgren H, Borga L (eds): Artificial Neural Networks in Medicine and Biology. London, United Kingdom, Springer-Verlag, 2000, pp 93-98
20. Wedeking P, Eaton S, Covell DG, et al: Pharmacokinetic analysis of blood distribution of intravenously administered 153Gd-labeled Gd-(DTPA)2- and 99mTc(DTPA) in rats. Magn Reson Imaging 8:567-575, 1990
21. Galbraith SM, Lodge M, Taylor NJ, et al: Reproducibility of dynamic contrast enhanced MRI in humans: Comparison of quantitative and semi-quantitative analysis. NMR Biomed 15:132-142, 2002
22. Parker GJ, Suckling J, Tanner SF, et al: Probing tumor microvascularity by measurement, analysis and display of contrast agent uptake kinetics. J Magn Reson Imaging 7:564-574, 1997
23. de Certaines JD, Henriksen O, Spisni A, et al: In vivo measurements of proton relaxation times in human brain, liver, and skeletal muscle: A multicenter MRI study. Magn Reson Imaging 11:841-850, 1993
24. Donahue KM, Burstein D, Manning WJ, et al: Studies of Gd-DTPA relaxivity and proton exchange rates in tissue. Magn Reson Med 32:66-76, 1994
25. Evelhoch JL: Key factors in the acquisition of contrast kinetic data for oncology. J Magn Reson Imaging 10:254-259, 1999
26. Weinmann HJ, Laniado M, Mutzel W: Pharmacokinetics of Gd-DTPA/dimeglumine after intravenous injection into healthy volunteers. Physiol Chem Phys Med NMR 16:167-172, 1984
27. Bland JM, Altman D: Measurement error proportional to the mean. BMJ 313:106, 1996
28. Padhani A, Gapinski C, Macvicar D, et al: Dynamic contrast enhanced MRI of prostate cancer: Correlation with morphology and tumor stage, histological grade and PSA. Clin Radiol 55:99-109, 2000
29. Hunter GJ, Hamberg LM, Choi N, et al: Dynamic T1-weighted magnetic resonance imaging and positron emission tomography in patients with lung cancer: Correlating vascular physiology with glucose metabolism. Clin Cancer Res 4:949-955, 1998
30. Horsman MR, Murata R, Breidahl T, et al: Combretastatin's novel vascular targeting drugs for improving anti-cancer therapy: Combretastatins and conventional therapy. Adv Exp Med Biol 476:311-323, 2000
31. Beauregard DA, Thelwall PE, Chaplin DJ, et al: Magnetic resonance imaging and spectroscopy of combretastatin A4 prodrug-induced disruption of tumor perfusion and energetic status. Br J Cancer 77:1761-1767, 1998
32. Beauregard DA, Hill SA, Chaplin DJ, et al: The susceptibility of tumors to the antivascular drug combretastatin A4 phosphate correlates with vascular permeability. Cancer Res 61:6811-6815, 2001
33. Su MY, Jao JC, Nalcioglu O: Measurement of vascular volume fraction and blood-tissue permeability constants with a pharmacokinetic model: Studies in rat muscle tumors with dynamic Gd-DTPA enhanced MRI. Magn Reson Med 32:714-724, 1994
34. Tofts PS: Modeling tracer kinetics in dynamic Gd-DTPA MR imaging. J Magn Reson Imaging 7:91-101, 1997
35. Buckley DL: Uncertainty in the analysis of tracer kinetics using dynamic contrast-enhanced T1-weighted MRI. Magn Reson Med 47:601-606, 2002
36. Landis CS, Li X, Telang FW, et al: Determination of the MRI contrast agent concentration time course in vivo following bolus injection: Effect of equilibrium transcytolemmal water exchange. Magn Reson Med 44:563-574, 2000
37. Buckley DL: Transcytolemmal water exchange and its affect on the determination of contrast agent concentration in vivo. Magn Reson Med 47:420-424, 2002
38. Stanisz GJ, Henkelman RM: Gd-DTPA relaxivity depends on macromolecular content. Magn Reson Med 44:665-667, 2000

39. Rijpkema M, Kaanders JH, Joosten FB, et al: Method for quantitative mapping of dynamic MRI contrast agent uptake in human tumors. J Magn Reson Imaging 14:457-463, 2001

40. Dowlati A, Robertson K, Cooney M, et al: A phase I pharmacokinetic and translational study of the novel vascular targeting agent combretastatin A-4 phosphate on a single-dose intravenous schedule in patients with advanced cancer. Cancer Res 62:3408-3416, 2002

41. Parkins CS, Dennis MF, Stratford MR, et al: Ischemia reperfusion injury in tumors: The role of oxygen radicals and nitric oxide. Cancer Res 55:6026-6029, 1995

42. Parkins C, Holder A, Hill S, et al: Determinants of anti-vascular action by combretastatin A-4 phosphate: Role of nitric oxide. Br J Cancer 83:811-816, 2000

43. Suzuki M, Hori K, Abe I, et al: A new approach to cancer chemotherapy: Selective enhancement of tumor blood flow with angiotensin II. J Natl Cancer Inst 67:663-669, 1981

44. Burton MA, Gray BN, Self GW, et al: Manipulation of experimental rat and rabbit liver tumor blood flow with angiotensin II. Cancer Res 45:5390-5393, 1985

45. Voorhees WD 3rd, Babbs CF: Hydralazine-enhanced selective heating of transmissible venereal tumor implants in dogs. Eur J Cancer Clin Oncol 18:1027-1033, 1982

46. Horsman MR, Christensen KL, Overgaard J: Relationship between the hydralazine-induced changes in murine tumor blood supply and mouse blood pressure. Int J Radiat Oncol Biol Phys 22:455-458, 1992

47. Grosios K, Holwell SE, McGown AT, et al: In vivo and in vitro evaluation of combretastatin A-4 and its sodium phosphate prodrug. Br J Cancer 81:1318-1327, 1999

48. Galbraith SM, Chaplin D, Lee F, et al: Effects of combretastatin A4 phosphate on endothelial cell shape in vitro and relation to vascular targeting effects in vivo. Anticancer Res 21:93-102, 2001

49. Kanthou C, Tozer GM: The tumor vascular targeting agent combretastatin A-4-phosphate induces reorganization of the actin cytoskeleton and early membrane blebbing in human endothelial cells. Blood 99:2060-2069, 2002

50. Tozer GM, Prise VE, Wilson J, et al: Mechanisms associated with tumor vascular shutdown induced by combretastatin A-4 phosphate: Intravital microscopy and measurement of vascular permeability. Cancer Res 61:6413-6422, 2001

51. Baxter LT, Jain RK: Transport of fluid and macromolecules in tumors: I. Role of interstitial pressure and convection. Microvasc Res 37:77-104, 1989

52. Baxter LT, Jain RK: Transport of fluid and macromolecules in tumors: II. Role of heterogeneous perfusion and lymphatics. Microvasc Res 40:246-263, 1990

53. Griffon-Etienne G, Boucher Y, Brekken C, et al: Taxane-induced apoptosis decompresses blood vessels and lowers interstitial fluid pressure in solid tumors: Clinical implications. Cancer Res 59:3776-3782, 1999

54. Milosevic MF, et al: Interstitial fluid pressure in cervical carcinoma: Within tumor heterogeneity, and relation to oxygen tension. Cancer 82:2418-2426, 1998

55. Milosevic MF, Fyles AW, Hill RP: The relationship between elevated interstitial fluid pressure and blood flow in tumors: A bioengineering analysis. Int J Radiat Oncol Biol Phys 43:1111-1123, 1999

56. Malek AM, Lee IW, Alper SL, et al: Regulation of endothelin-1 gene expression by cell shape and the microfilament network in vascular endothelium. Am J Physiol 273:C1764-C1774, 1997

57. Morita T, Kurihara H, Maemura K, et al: Disruption of cytoskeletal structures mediates shear stress-induced endothelin-1 gene expression in cultured porcine aortic endothelial cells. J Clin Invest 92:1706-1712, 1993

58. Ozawa F, Kasuya Y, Hama H, et al: Microtubule dynamics regulates the level of endothelin-B receptor in rat cultured astrocytes. J Neurochem 69:562-569, 1997

59. Gibbons G: Endothelial function as a determinant of vascular function and structure: A new therapeutic target. Am J Cardiol 79:3-8, 1997